

# New Space Vector Selection Scheme for VSI Supplied Dual Three-Phase Induction Machine

Dragan MILIĆEVIĆ<sup>1</sup>, Vladimir KATIĆ<sup>1</sup>, Zoltan ČORBA<sup>1</sup>, Marian GRECONICI<sup>2</sup>

<sup>1</sup>University of Novi Sad, Faculty of Technical Sciences, Novi Sad, Serbia

<sup>2</sup>Politehnica University of Timisoara, Physical Foundation of Engineering Dept., Timisoara, Romania  
milicevd@uns.ac.rs, katav@uns.ac.rs, zobos@uns.ac.rs, marian.greconici@et.upt.ro

**Abstract**—This paper presents a novel space vector selection scheme applicable for the control of dual three-phase induction motor drives supplied from a six-phase voltage source inverter (VSI). The vector selection method is based on the vector space decomposition technique (VSD). Unique vector selection pattern simplifies problems related to complicated implementation of standard VSD in commercially available digital signals processors (DSP). The proposed vector selection scheme is verified through a theoretical analysis, computer simulations and practical experimental results conducted on a dual three-phase test rig prototype with control algorithm implemented in Texas Instrument's TMS320F2808 DSP.

**Index Terms**—digital signal processor, dual three-phase induction motor, space vector pulse width modulation, vector space decomposition, voltage source inverter.

## I. INTRODUCTION

Motor drives featuring high reliability, prominent immunity to failures and low torque ripple are typical applications in which multiphase machines have primacy over the standard three-phase machines [1-3]. Taking into account that the multiphase approach allows reduction of the required rating of power electronic components, it becomes clear why multiphase machines are the preferred choice for high power / high performance / high efficiency / high reliability drives, such as drives for electric ship propulsion [4], railway traction [5], “more electric” aircraft applications, high power winders for paper and textile industry, etc.

One of the most interesting and most investigated multiphase machines are dual three-phase machines that have two three phase winding sets spatially shifted by 30 electrical degrees. The analysis based on a space vector approach shows that the mathematical model of dual three-phase machine can be transformed from the original phase-variable six-dimensional domain to three decoupled perpendicular subspaces [1]. Apart from being decoupled, among the set of subspaces there is only one wherein the torque / flux producing variables are mapped. In the remaining two subspaces only losses manifest so they do not contribute in the process of electromechanical energy conversion.

Because of these specific characteristics, the main concern in typical application of VSI fed dual three-phase machine is how to avoid or minimize the generation of components in the loss manifesting subspaces.

Furthermore, considering the hardware and software PWM implementation complexity, it can be stated that driving of the six-phase inverter is a challenging task.

Different approaches were developed in the past to deal with these specific requirements. The comprehensive analysis and comparative study presented in [6] and [7], showed that it is difficult to simultaneously satisfy these two essential criteria – the PWM implementation complexity and loss minimization. It is demonstrated that a conventional space vector modulation (SVM) [8], while easy to implement in standard DSP, is not capable of dealing with extra loss production. A much better loss attenuation effect can be achieved using the VSD technique, originally presented in [9]. Digital implementation complexity is identified as the VSD major drawback. A compromise between the demands for reduction of implementation complexity and losses generation can be achieved using the vector classification [10] and double zero-sequence injection technique [11].

A breakthrough was made by K. Marouani, L. Baghli, D. Hadiouche, A. Kheloui and A. Rezzoug [12]. It is shown that an adequate vector arrangement can dramatically improve dual three-phase machine exploitation characteristics in terms of loss minimization and, at the same time, can lead to the control system simplification. It is proven that only zero vector placements (at the beginning or at the end of the PWM cycle) can provoke an additional loss decrease or increase.

This paper introduces the novel vector selection scheme PWM method based on the space vector approach for dual three-phase induction machine drives. Considering that 64 different inverter switching configurations offer a numerous applicable vector combinations it is shown that the presented vector pattern can effectively and simultaneously satisfy two major criteria – the limitation of additional losses and the ease of implementation.

The simulation and experimental results conducted on the dual three-phase test rig are provided to demonstrate the validity and quality of proposed technique.

## II. MACHINE MODEL

The mathematical model of the dual three-phase machine is developed using the VSD theory. Only the basic set of equations is presented in order to outline the fundamental characteristics of the machine model in the original (2), (3) and decoupled system (4), (5), (6). A detailed machine model can be found in [9] and [13].

After applying the amplitude invariant VSD

transformation matrix (1), presented in [11], to the stator and rotor voltage equations (2) and (3), the original six-dimensional machine system can be decomposed into three two-dimensional orthogonal (decoupled) subspaces with the following characteristics:

- Flux/torque producing  $\alpha$ - $\beta$  subspace contains the fundamental components of machine variables and the harmonics of the order  $k=12n\pm1$  ( $n=1,2,3,\dots$ ) as given by the equation (4) shown at the bottom of the page,
- Loss producing (non flux/torque producing)  $\mu_1$ - $\mu_2$  subspace contains harmonics of the order  $k=6n\pm1$  ( $n=1,3,5,\dots$ ) given by the equation (5) shown at the bottom of the page,
- Zero-sequence  $z_1$ - $z_2$  subspace contains zero-sequence components. In topology where two three phase windings are wye-connected with isolated neutrals, the  $z_1$ - $z_2$  subspace components are equal to zero.

The vectors and matrices used in (2), (3), (4) and (5) are given and described in the Appendix of [11].

$$T_6 = \frac{1}{3} \begin{bmatrix} 1 & -\frac{1}{2} & -\frac{1}{2} & \frac{\sqrt{3}}{2} & -\frac{\sqrt{3}}{2} & 0 \\ 0 & \frac{\sqrt{3}}{2} & -\frac{\sqrt{3}}{2} & \frac{1}{2} & \frac{1}{2} & -1 \\ 1 & -\frac{1}{2} & -\frac{1}{2} & -\frac{\sqrt{3}}{2} & \frac{\sqrt{3}}{2} & 0 \\ 0 & \frac{\sqrt{3}}{2} & \frac{\sqrt{3}}{2} & \frac{1}{2} & \frac{1}{2} & -1 \\ 1 & \frac{1}{2} & \frac{1}{2} & 0 & 0 & 0 \\ 0 & 0 & 0 & 1 & 1 & 1 \end{bmatrix} \quad (1)$$

$$\begin{bmatrix} v_s \end{bmatrix} = \begin{bmatrix} R_s \end{bmatrix} \begin{bmatrix} i_s \end{bmatrix} + \frac{d}{dt} \begin{bmatrix} \psi_s \end{bmatrix} = \quad (2)$$

$$= \begin{bmatrix} R_s \end{bmatrix} \begin{bmatrix} i_s \end{bmatrix} + \frac{d}{dt} \left\{ \begin{bmatrix} L_{ss} \end{bmatrix} \begin{bmatrix} i_s \end{bmatrix} + \begin{bmatrix} L_{sr} \end{bmatrix} \begin{bmatrix} i_r \end{bmatrix} \right\}$$

$$\begin{bmatrix} v_r \end{bmatrix} = 0 = \begin{bmatrix} R_r \end{bmatrix} \begin{bmatrix} i_r \end{bmatrix} + \frac{d}{dt} \begin{bmatrix} \psi_r \end{bmatrix} = \quad (3)$$

$$= \begin{bmatrix} R_r \end{bmatrix} \begin{bmatrix} i_r \end{bmatrix} + \frac{d}{dt} \left\{ \begin{bmatrix} L_{rr} \end{bmatrix} \begin{bmatrix} i_r \end{bmatrix} + \begin{bmatrix} L_{rs} \end{bmatrix} \begin{bmatrix} i_s \end{bmatrix} \right\}$$

The electromagnetic torque in stationary reference frame  $\alpha, \beta$  can be expressed as [11]:

$$T_e = 3 \frac{P}{2} \frac{M}{L_r} \left( \psi_{\alpha r} i_{\beta s} - \psi_{\beta r} i_{\alpha s} \right) \quad (6)$$

$$\begin{bmatrix} v_{\alpha s} \\ v_{\beta s} \\ 0 \\ 0 \end{bmatrix} = \begin{bmatrix} R_s + (L_{ls} + M)p & 0 & Mp & 0 \\ 0 & R_s + (L_{ls} + M)p & 0 & Mp \\ Mp & \omega_r M & R_r' + (L_{lr}' + M)p & \omega_r (L_{lr}' + M) \\ -\omega_r M & Mp & -\omega_r (L_{lr}' + M) & R_r' + (L_{lr}' + M)p \end{bmatrix} \begin{bmatrix} i_{\alpha s} \\ i_{\beta s} \\ i_{\alpha r} \\ i_{\beta r} \end{bmatrix} \quad (4)$$

$$\begin{bmatrix} v_{\mu_1 s} \\ v_{\mu_2 s} \\ 0 \\ 0 \end{bmatrix} = \begin{bmatrix} R_s + L_{ls}p & 0 & 0 & 0 \\ 0 & R_s + L_{ls}p & 0 & 0 \\ 0 & 0 & R_r + L_{lr}p & 0 \\ 0 & 0 & 0 & R_r + L_{lr}p \end{bmatrix} \begin{bmatrix} i_{\mu_1 s} \\ i_{\mu_2 s} \\ i_{\mu_1 r} \\ i_{\mu_2 r} \end{bmatrix} \quad (5)$$

### III. INTRODUCTION OF NEW VECTOR SELECTION PATTERN

#### A. Six phase inverter analysis

The analysis of six phase inverter shows  $2^6$  (64) different switching configurations (naturally, shoot-through states are excluded) [14].

Referred to Fig. 2, the machine phase voltages can be expressed in the matrix form (7). Applying the VSD transformation matrix (1) on (7), the machine phase voltage matrix can be decomposed into  $\alpha$ - $\beta$ ,  $\mu_1$ - $\mu_2$  and  $z_1$ - $z_2$  subspace voltage vectors.

$$\begin{bmatrix} v_0 \\ v_a \\ v_x \\ v_b \\ v_y \\ v_c \\ v_z \end{bmatrix} = \frac{1}{6} \begin{bmatrix} 2 & 0 & 2 & 0 & 2 & -2 & 2 \\ 4 & 4 & 2 & 2 & 0 & 2 & 0 \\ 0 & 4 & 4 & 2 & 2 & 0 & 2 \\ -2 & -2 & 2 & 2 & 0 & 2 & 0 \\ 0 & -2 & -2 & 2 & 2 & 0 & 2 \\ -2 & -2 & -4 & -4 & 0 & 2 & 0 \\ 0 & -2 & -2 & -4 & -4 & 0 & 2 \end{bmatrix} \begin{bmatrix} v_{AN} - v_{XN} \\ v_{XN} - v_{BN} \\ v_{BN} - v_{YN} \\ v_{YN} - v_{CN} \\ v_{CN} - v_{ZN} \\ 0 \\ 0 \end{bmatrix} \quad (7)$$

The projection of voltage vectors in the  $\alpha$ - $\beta$  and  $\mu_1$ - $\mu_2$  subspaces is illustrated in Fig. 3. The vector numbers are formed from the inverter switching state, namely, its binary equivalent number gives the value of the switching functions for the inverter legs, given in the following order ZYXCBA (the most significant bit is Z).

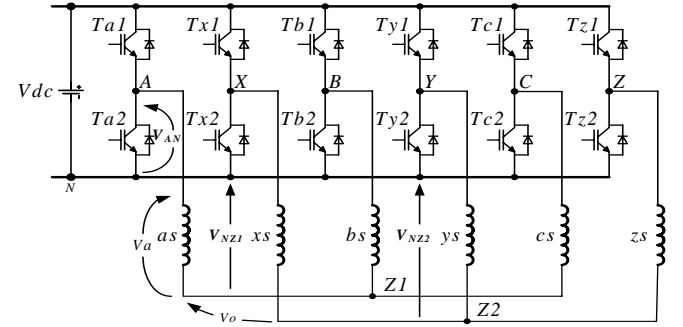


Figure 2. Winding arrangement of dual three-phase induction machine

#### B. New vector selection pattern

The objective of SVM is to supply voltages to the machine in accordance with the reference voltage vector generated by the control system. Also, it is preferred that the modulator used for dual three-phase machine has unique characteristics such as:

- Ease of PWM switching pattern implementation,
- Taking into consideration existence of multiple planes (as mentioned before, only  $\alpha$ - $\beta$  subspace components are responsible for flux/torque producing currents).

The VSD technique approach divides  $\alpha$ - $\beta$  subspace in 12 sectors [9]. According to the VSD, one zero and four largest non-zero voltage vectors, which are nearest to the reference vector, are chosen so that the following equation has a unique and positive solution:

$$\begin{bmatrix} t_1 \\ t_2 \\ t_3 \\ t_4 \\ t_5 \end{bmatrix} = \begin{bmatrix} v_1^\alpha & v_2^\alpha & v_3^\alpha & v_4^\alpha & v_5^\alpha \\ v_1^\beta & v_2^\beta & v_3^\beta & v_4^\beta & v_5^\beta \\ v_1^{\mu 1} & v_2^{\mu 1} & v_3^{\mu 1} & v_4^{\mu 1} & v_5^{\mu 1} \\ v_1^{\mu 2} & v_2^{\mu 2} & v_3^{\mu 2} & v_4^{\mu 2} & v_5^{\mu 2} \\ 1 & 1 & 1 & 1 & 1 \end{bmatrix}^{-1} \begin{bmatrix} v_{s\alpha}^* \\ v_{s\beta}^* \\ 0 \\ 0 \\ 1 \end{bmatrix} T_s \quad (8)$$

where  $t_i$  is the time interval within sampling period  $T_s$  during which vector  $V_i$  is applied,  $i=1,2,3,4,5$ . For example, if the reference vector is in the sector 1 (the sector bounded by vectors  $V_9$  and  $V_{11}$  in Fig. 3. in  $\alpha$ - $\beta$  subspace), the VSD technique will use four large vectors  $V_{41}$ ,  $V_9$ ,  $V_{11}$  and  $V_{27}$ .

The similar duty ratio calculation principle is used in new modulation technique. The major difference between these two techniques lies in the vector selection scheme.

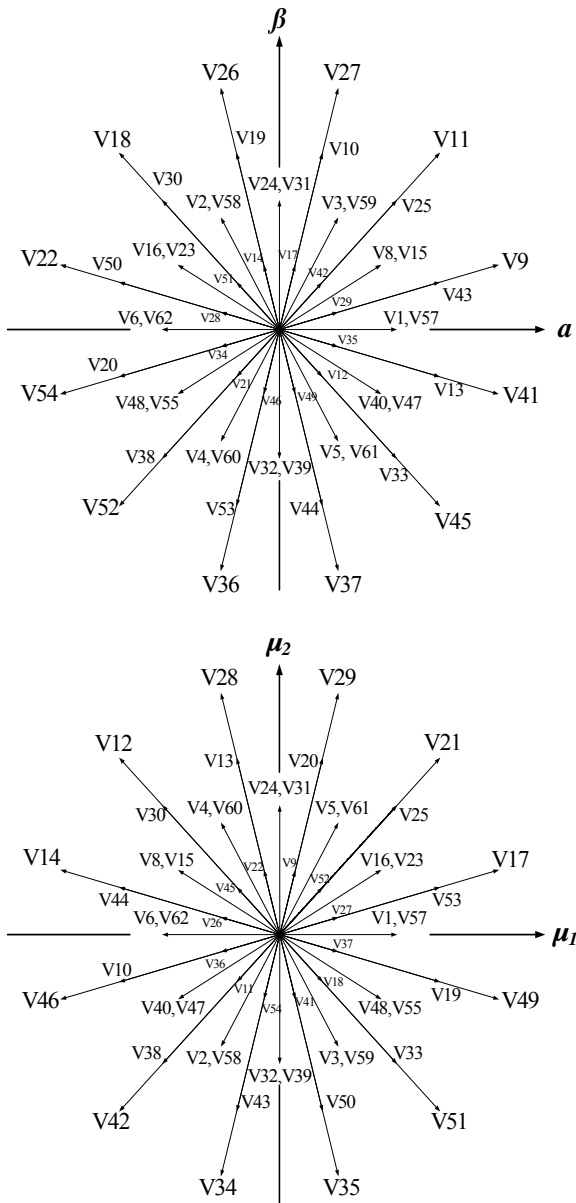


Figure 3. Inverter voltage vectors in  $\alpha$ - $\beta$  and  $\mu_1$ - $\mu_2$  subspace

For example, assuming that the reference vector lies in the Sector 1P (Sectors are signed as 1P, 1S, 2P...12S as in Fig. 4.), the modulator will select large vectors  $V_{45}$ ,  $V_{41}$ ,  $V_9$  and one medium vector  $V_8$ , (Fig. 3.) while if the reference voltage vector is positioned in the Sector 1S then the algorithm will select large vectors  $V_{41}$ ,  $V_9$ ,  $V_{11}$  and one medium vector  $V_{40}$ , etc.

The motivation for the new vector selecting pattern proposal can be explained by analyzing the PWM signals of VSD and proposed technique depicted in Fig.5. The dashed line shows the PWM output signals for the case of original VSD when the reference vector lies in the Sector 1, while the continuous line shows the PWM signals provided by the proposed technique (the reference vector lies in the Sector 1S). It is clear that the VSD switching function for channel B has to be obtained by the special PWM modulators since it requires six commutations in the same PWM cycle, while remaining legs will bare only two commutations. The new modulation technique overcomes this problem by a different vector selection scheme in the process of approximation of the reference vector.

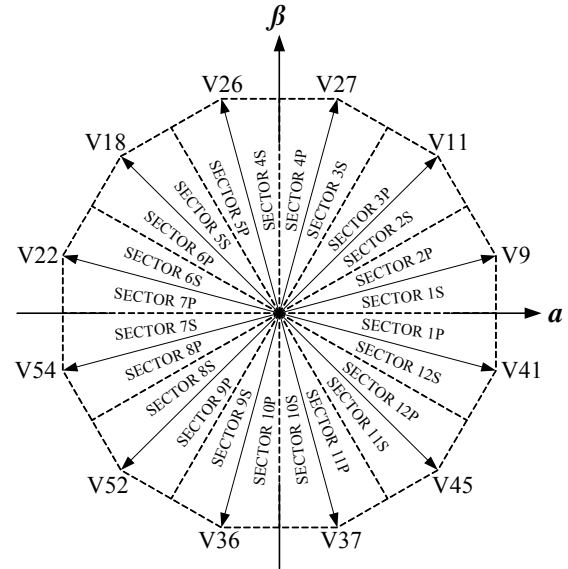


Figure 4. 24 sectors in  $\alpha$ - $\beta$  plain

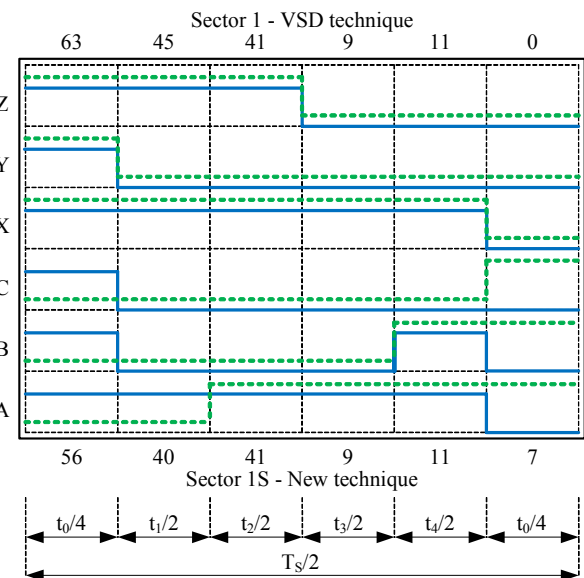


Figure 5. New technique (continuous) and VSD technique (dashed) PWM signals

### C. DSP implementation guide

The optimal DSP implementation implies the reduction of computational effort needed to solve the equation (8). Therefore, an off-line calculation has to be undertaken. The steps for the DSP software simplification, presented in this paper, are based on the analysis given in [9], [12] and [15].

To avoid the complex inverse 5x5 matrix calculation, a theoretical analysis has shown that only 12 coefficients in every PWM cycle have to be calculated using the equation (9).

$$\begin{bmatrix} T_1 \\ T_2 \\ T_3 \\ T_4 \\ T_5 \\ T_6 \\ T_7 \\ T_8 \\ T_9 \\ T_{10} \\ T_{11} \\ T_{12} \end{bmatrix} = \frac{\sqrt{3}}{2} \frac{T_s}{V_{DC}} \begin{bmatrix} 0 & -2 \\ 1 & 2-\sqrt{3} \\ \sqrt{3}-1 & \sqrt{3}-1 \\ 2-\sqrt{3} & 1 \\ -2 & 0 \\ 2-\sqrt{3} & -1 \\ \sqrt{3}-1 & -(\sqrt{3}-1) \\ 1 & -\sqrt{3} \\ -\sqrt{3} & -1 \\ 1 & -(2-\sqrt{3}) \\ \sqrt{3} & -1 \\ -1 & -\sqrt{3} \end{bmatrix} \begin{bmatrix} v_{s\alpha}^* \\ v_{s\beta}^* \end{bmatrix} \quad (9)$$

A different vector selection pattern compared to the selection scheme presented in [12] and the use of amplitude invariant transformation matrix (1) result in a different duty time ratio equation. Four corresponding pairs of duty time and non-zero vectors for each sector can be found using the equation (9) and Table I. The remaining zero vector is selected in such a manner that only one transition occurs (low to high or high to low depending on the position of reference vector i.e. active sector) at each PWM channel. Time superscripts in each cell of Table I, indicate which vector must be applied during the corresponding duty ratio time. For example, assume that the reference vector is located in the Sector 1S. Using the equation (9), coefficients  $T_1$  to  $T_{12}$  need to be calculated. From Table I it can be found that the active vectors to be used for the considered sector are V40 for period  $T_6$ , V41 for period  $T_7$ , V9 for period  $T_{10}$  and V11 for period  $T_1$  (note that the equation (4) for the sector 1S would give negative value of  $T_1$ ).

### IV. SIMULATION RESULTS

The validity of theoretical analysis is proven by means of simulations using MATLAB Simulink.

On the control side, the simplest open-loop V/f control is applied. Motor phase voltages and their spectrum, motor phase currents and  $\alpha$ - $\beta$  and  $\mu_1$ - $\mu_2$  subspace current trajectories are presented in Fig. 6. The frequency reference is set to 35 Hz and PWM switching frequency is 5 kHz.

Fig. 6a and Fig. 6b confirm that the inverter voltages are accurately generated, namely their THD is below 2.5 % and their mutual phase shift is as expected (waveforms of phase pairs A, B, C and X, Y, Z are mutually shifted by  $\pi/6$  and phase shift between phases in each winding group is  $2\pi/3$ ).

The trajectories of  $\alpha$ - $\beta$  and  $\mu_1$ - $\mu_2$  subspace currents, presented in Fig. 6d, are calculated from motor phase currents (presented in Fig. 6c) using transformation (1). A

pure circular shape of  $\alpha$ - $\beta$  trajectory and more than sixty times mitigated  $\mu_1$ - $\mu_2$  subspace components are another evidence of the PWM method regularity.

### V. EXPERIMENTAL RESULTS

Experiments are conducted on a custom made test rig shown in Fig. 7. The test rig consist of dual three-phase motor, six phases VSI and control card with additional analog and digital interface boards.

The power segment of six phase inverter is formed using six Semikron half-bridge IGBT modules SKM 50GB123D controlled by SKHI 22A IGBT drivers. Inverter output currents are measured by current sensors LEM LA55. The eZDSP development system, based on stand-alone Texas Instrument's TMS320F2808 DSP, is used as a control unit. The nameplate data of the six pole dual three-phase motor are as follows: 1.1 kW, 1.75 A, 400 V, 50 Hz.

Again, for experimental purposes, the simplest V/f control method is implemented in DSP [16].

For 35 Hz fundamental harmonic reference, the motor phase currents are presented in Fig. 8a. According to the mutual phase shift of waveforms it can be stated that the motor phase currents are generated correctly.

On the other hand, Fig. 8b shows that  $\mu_1$ - $\mu_2$  components attenuation effect is not significant as in the simulation -  $\mu_1$ - $\mu_2$  components are about fifteen times lower than  $\alpha$ - $\beta$  components. An explanation lies in the fact that there are some construction differences between the real machine and simulated one.

TABLE I. DUTY RATIO TIME CALCULATION ACCORDING TO SECTOR

		$tV_1$	$tV_2$	$tV_3$	$tV_4$
<b>SECTOR</b>	<b>1P</b>	$T_1^{V45}$	$T_2^{V41}$	$T_3^{V9}$	$T_4^{V8}$
	<b>1S</b>	$T_6^{V40}$	$T_7^{V41}$	$T_{10}^{V9}$	$-T_1^{V11}$
	<b>2P</b>	$T_8^{V41}$	$T_3^{V9}$	$T_4^{V11}$	$-T_6^{V3}$
	<b>2S</b>	$T_7^{V1}$	$T_{10}^{V9}$	$T_2^{V11}$	$-T_8^{V27}$
	<b>3P</b>	$T_{11}^{V9}$	$T_4^{V11}$	$-T_6^{V27}$	$-T_7^{V31}$
	<b>3S</b>	$T_{10}^{V15}$	$T_2^{V11}$	$T_3^{V27}$	$-T_{11}^{V26}$
	<b>4P</b>	$-T_5^{V11}$	$-T_6^{V27}$	$-T_7^{V26}$	$-T_{10}^{V58}$
	<b>4S</b>	$T_2^{V59}$	$T_3^{V27}$	$T_4^{V26}$	$T_5^{V18}$
	<b>5P</b>	$-T_9^{V27}$	$-T_7^{V26}$	$-T_{10}^{V18}$	$-T_2^{V16}$
	<b>5S</b>	$T_3^{V24}$	$T_4^{V26}$	$-T_6^{V18}$	$T_9^{V22}$
	<b>6P</b>	$-T_{12}^{V26}$	$-T_{10}^{V18}$	$-T_2^{V22}$	$-T_3^{V6}$
	<b>6S</b>	$T_4^{V2}$	$-T_6^{V18}$	$-T_7^{V22}$	$T_{12}^{V54}$
<b>SECTOR</b>	<b>7P</b>	$-T_1^{V18}$	$-T_2^{V22}$	$-T_3^{V54}$	$-T_4^{V55}$
	<b>7S</b>	$-T_6^{V23}$	$-T_7^{V22}$	$-T_{10}^{V54}$	$T_1^{V52}$
	<b>8P</b>	$-T_8^{V22}$	$-T_3^{V54}$	$-T_4^{V52}$	$T_6^{V60}$
	<b>8S</b>	$-T_7^{V62}$	$-T_{10}^{V54}$	$-T_2^{V52}$	$T_8^{V36}$
	<b>9P</b>	$-T_{11}^{V54}$	$-T_4^{V52}$	$T_6^{V36}$	$T_7^{V32}$
	<b>9S</b>	$-T_{10}^{V48}$	$-T_2^{V52}$	$-T_3^{V36}$	$T_{11}^{V37}$
	<b>10P</b>	$T_5^{V52}$	$T_6^{V36}$	$T_7^{V37}$	$T_{10}^{V5}$
	<b>10S</b>	$-T_2^{V4}$	$-T_3^{V36}$	$-T_4^{V37}$	$-T_5^{V45}$
	<b>11P</b>	$T_9^{V36}$	$T_7^{V37}$	$T_{10}^{V45}$	$T_2^{V47}$
	<b>11S</b>	$-T_3^{V39}$	$-T_4^{V37}$	$T_6^{V45}$	$-T_9^{V41}$
	<b>12P</b>	$T_{12}^{V37}$	$T_{10}^{V45}$	$T_2^{V41}$	$T_3^{V57}$
	<b>12S</b>	$-T_4^{V61}$	$T_6^{V45}$	$T_7^{V41}$	$-T_{12}^{V9}$

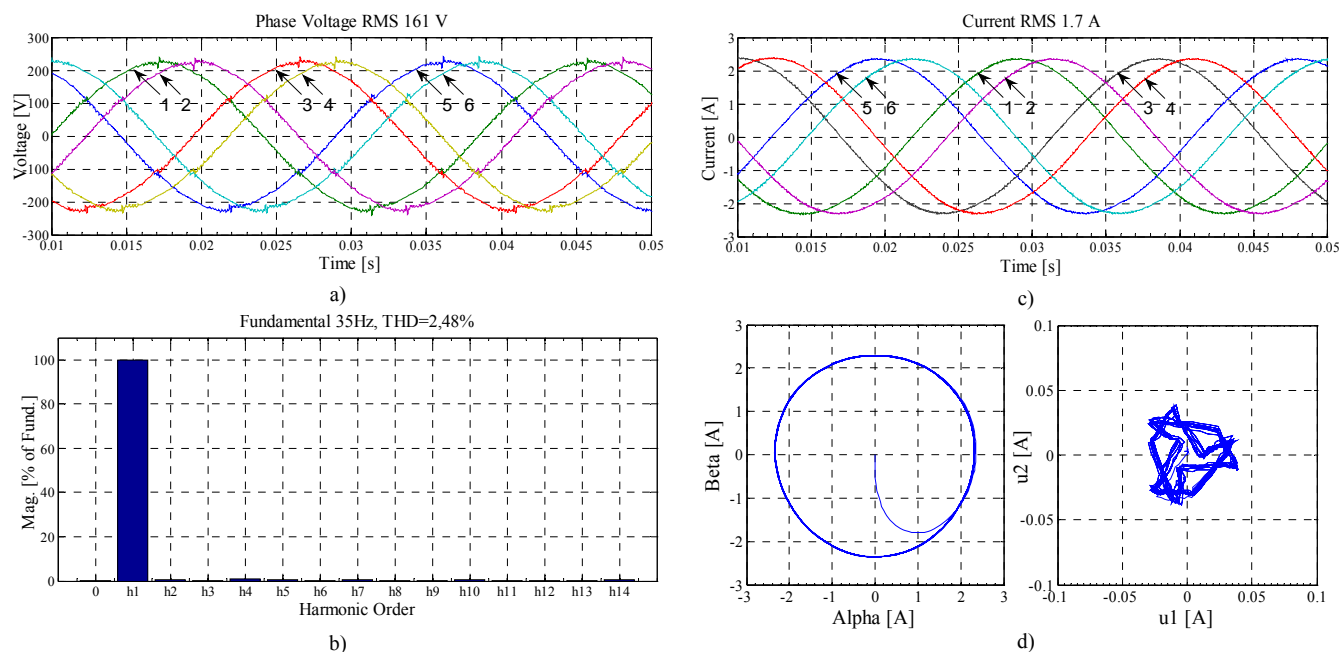


Figure 6. Simulation results a) Dual three-phase motor phase voltages (1- Phase voltage  $V_a$ , 2- Phase voltage  $V_x$ , 3- Phase voltage  $V_b$ , 4- Phase voltage  $V_y$ , 5- Phase voltage  $V_c$ , 6- Phase voltage  $V_z$ ), b) Phase A inverter output harmonic spectrum, c) Dual three-phase motor currents (1- Phase A current, 2- Phase X current, 3- Phase B current, 4- Phase Y current, 5- Phase C current, 6- Phase Z current), d)  $\alpha$ - $\beta$  and  $\mu_1$ - $\mu_2$  current trajectories



Figure 7. Experimental test rig

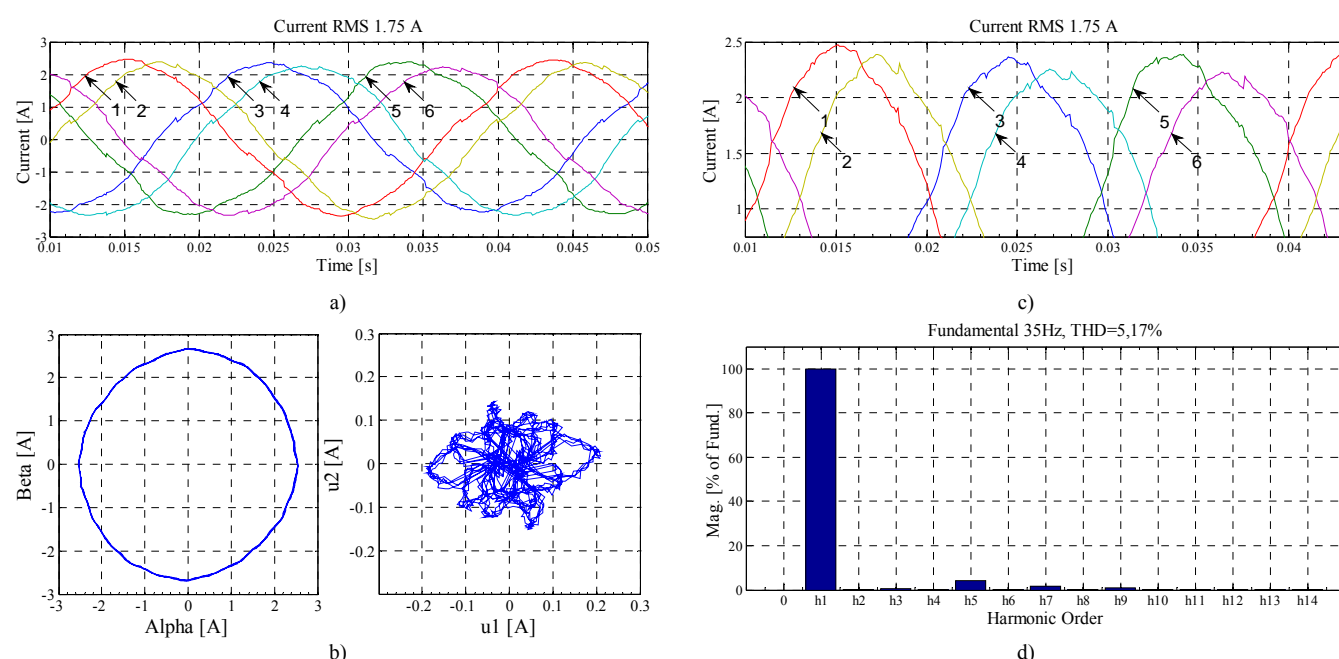


Figure 8. Experimental results a) Dual three-phase motor currents (1- Phase A current, 2- Phase X current, 3- Phase B current, 4- Phase Y current, 5- Phase C current, 6- Phase Z current), b)  $\alpha$ - $\beta$  and  $\mu_1$ - $\mu_2$  current trajectories, c) Enlarged segment of phase currents waveform (1- Phase A current, 2- Phase X current, 3- Phase B current, 4- Phase Y current, 5- Phase C current, 6- Phase Z current), d) Motor phase A current harmonic spectrum

The motor windings asymmetry, which exists in the real machine and is not introduced in the simulation, is recognized as the major factor which causes the difference [17-21]. The practical aspect of noticed asymmetry is manifested through the RMS values difference between the motor phase currents: amplitudes and consequently the RMS values of phase currents are not equal:  $I_{Apeak}=2.48$  A,  $I_{Bpeak}=2.37$  A,  $I_{Cpeak}=2.39$  A,  $I_{Xpeak}=2.39$  A,  $I_{Ypeak}=2.26$  A,  $I_{Zpeak}=2.23$  A. The current asymmetry, evident from an enlarged part of Fig. 8a, is shown in Fig. 8c. The difference is even visible in the currents of the same three phase winding group.

Another evident impact of machine construction imbalance on the PWM technique performance is visible in the phase current harmonic spectrum shown in Fig. 8d. From Fig. 8d the existence of 5th and 7th harmonics, related to  $\mu_1$ - $\mu_2$  subspace, is noticeable.

## VI. CONCLUSION

In this paper, a space vector modulation method for dual three-phase induction machine based on a novel vector selection scheme has been investigated. The presented method is based on the VSD technique but, unlike the original, beside long vectors it uses middle size vectors for correct reference approximation. The adopted vector selection pattern and presented off-line calculation principles, which reduce the software complexity and computation time, make a DSP implementation possible and at the same time provide an additional loss minimization effect.

The regularity of theoretical analysis is verified through simulations and experiments and a good compliance is achieved.

There, it is also noticed that the crucial concern using this and similar types of PWM techniques is related to the dual three-phase motor design. The motor asymmetry will lead to the generation of unwanted  $\mu_1$ - $\mu_2$  subspace components responsible for additional motor losses.

## REFERENCES

- [1] E. Levi, R. Bojoi, F. Profumo, H.A. Toliyat, and S. Williamson, "Multiphase induction motor drives - a technology status review," The Institution of Engineering Technology, IET, Electric Power Applications, EPA, vol. 1, no. 4, pp. 489-516, 2007. [Online]. Available: <http://dx.doi.org/10.1049/iet-epa:20060342>
- [2] E. Levi, "Multiphase Electric Machines for Variable-Speed Applications," IEEE Transaction on Industrial Electronics, Vol. 55, Issue 5, pp 1893-1909, 2008. [Online]. Available: <http://dx.doi.org/10.1109/TIE.2008.918488>
- [3] G. Singh, "Multi-phase induction machine drive research—a survey," Electric Power Systems Research, vol. 61, no. 2, pp. 139-147, Mar. 2002. [Online]. Available: [http://dx.doi.org/10.1016/S0378-7796\(02\)00007-X](http://dx.doi.org/10.1016/S0378-7796(02)00007-X)
- [4] S. Lu and K. Corzine, "Multilevel multi-phase propulsion drives," Proceedings of IEEE ESTS 2005, Philadelphia, PA, USA, pp. 363-370, 2005. [Online]. Available: <http://dx.doi.org/10.1109/ESTS.2005.1524701>
- [5] M. Steiner, R. Deplazes, and H. Stemmler, "A new transformerless topology for AC-fed traction vehicles using multi-star induction motors," EPE Journal, vol. 10, no. 3/4, pp. 45-53, 2000.
- [6] R. Bojoi, A. Tenconi, F. Profumo, G. Griva, and D. Martinello, "Complete Analysis and Comparative Study of Digital Modulation Techniques for Dual Three-Phase AC Motor Drives," Proceedings of IEEE Power Electronics Specialists Conference PESC, 33th Annual Meeting, Queensland, Australia, vol. 2, pp. 851-857, 2002. [Online]. Available: <http://dx.doi.org/10.1109/PSEC.2002.1022560>
- [7] R. Bojoi, F. Farina, F. Profumo and, A. Tenconi, "Dual-Three Phase Induction Machine Drives Control—A Survey," IEEE Transactions on Industry Applications, vol. 126, no. 4, pp. 420-429, 2006. [Online]. Available: <http://dx.doi.org/10.1541/ieejias.126.420>
- [8] K. Gopakumar, V.T. Ranganathan, and S.R. Bhat, "Split-Phase Induction Motor Operation from PWM Voltage Source Inverter," IEEE Transactions on Industry Applications, vol. 29, no.5, pp. 927-932, 1993. [Online]. Available: <http://dx.doi.org/10.1109/IAS.1991.178192>
- [9] Y. Zhao, and T.A. Lipo, "Space vector PWM control of dual three-phase induction machine using vector space decomposition," IEEE Transactions on Industry Application, vol. 31, pp. 1100-1108, 1995. [Online]. Available: <http://dx.doi.org/10.1109/IAS.1994.345429>
- [10] A.R. Bakhshai, G. Joos, and H. Jin, "Space Vector PWM Control of a Split-Phase Induction Machine Using The Vector Classification Technique," The 13th Annual Applied Power Electronics Conference and Exhibition, APEC, February 15-19, Anaheim, California, USA, vol. 2, pp. 802-808, 1998. [Online]. Available: <http://dx.doi.org/10.1109/APEC.1998.653990>
- [11] R. Bojoi, M. Lazzari, F. Profumo, and A. Tenconi, "Digital field-oriented control for dual three-phase induction motor drives," IEEE Transaction on Industry Application, vol. 39, no. 3, pp. 752-760, 2003. [Online]. Available: <http://dx.doi.org/10.1109/TIA.2003.811790>
- [12] K. Marouani, L. Baghli, D. Hadiouche, A. Kheloui, and A. Rezzoug, "A New PWM Strategy Based on a 24-Sector Vector Space Decomposition for a Six-Phase VSI-Fed Dual Stator Induction Motor," IEEE Transaction on Industrial Electronics, vol. 55, no. 5, pp 1910-1920, 2008. [Online]. Available: <http://dx.doi.org/10.1109/TIE.2008.918486>
- [13] R. Bojoi, A. Tenconi, and F. Profumo, "Digital synchronous frame current regulation for dual-three phase induction motor drive," Proceedings of IEEE Power Electronics Specialists Conference PESC, 34th Annual Meeting, Acapulco, Mexico, pp. 1475-1480, 2003. [Online]. Available: <http://dx.doi.org/10.1109/PESC.2003.1216804>
- [14] M. B. R. Correa, C. B. Jacobina, C. R. da Silva, A. M. N. Lima, and E. R. C. da Silva, "Vector and scalar modulation for six-phase voltage source inverters," Proceedings of IEEE Power Electronics Specialists Conference PESC, 34th Annual Meeting, Acapulco, Mexico, vol. 2, pp. 562-567, 2003. [Online]. Available: <http://dx.doi.org/10.1109/PESC.2003.1218117>
- [15] D. Hadiouche, L. Baghli, and A. Rezzoug, "Space vector PWM techniques for dual three-phase AC machine: analysis, performance evaluation and DSP implementation," Industry Applications Conference, 38th IAS Annual Meeting, Conference vol.1, pp. 648 - 655, 2003. [Online]. Available: <http://dx.doi.org/10.1109/IAS.2003.1257571>
- [16] H.A. Toliyat. DSP-Based Electromechanical Motion Control. CRC Press, pp. 223-232, 2004.
- [17] D. Hadiouche, H. Razik, and A. Rezzoug, "On the design of dual-stator windings for safe VSI fed AC machine drives," Proceedings of Industry Applications Conference IAS, 36th Annual Meeting, Chicago, Illinois, USA, vol. 2, pp. 1123-1130, 2001. [Online]. Available: <http://dx.doi.org/10.1109/IAS.2001.955624>
- [18] D. Hadiouche, H. Razik, and A. Rezzoug, "On the modeling and design of dual-stator windings to minimize circulating harmonic currents for VSI fed AC machines," IEEE Transaction on Industry Application, vol. 40, no. 2, pp. 506-515, 2004. [Online]. Available: <http://dx.doi.org/10.1109/TIA.2004.824511>
- [19] R. Bojoi, F. Farina, A. Tenconi, F. Profumo, and E. Levi, "Stationary frame digital current regulation for dual-three phase induction motor drives," Proceedings of IEEE Power Electronics Specialists Conference PESC, 35th Annual Meeting, Aachen, Germany, vol. 3, pp. 2121- 2127, 2004. [Online]. Available: <http://dx.doi.org/10.1109/PESC.2004.1355446>
- [20] M. Jones, S. N. Vukosavic, D. Dujic, and E. Levi, "A synchronous current control scheme for multiphase induction motor drives," IEEE Transaction on Energy Conversion, vol. 24, no. 4, pp. 860-868, 2009. [Online]. Available: <http://dx.doi.org/10.1109/TEC.2009.2025419>
- [21] D. G. Dorrell, C. Y. Leong, and R. A. McMahon, "Analysis and Performance Assessment of Six-Pulse Inverter-Fed Three-Phase and Six-Phase Induction Machines," IEEE Transactions on Industry Applications, vol. 42, no. 6, pp. 1487-1495, 2006. [Online]. Available: <http://dx.doi.org/10.1109/TIA.2006.882673>